Tampere University

Jesse Koskinen

RED-EMITTING MEMBRANE EXTERNAL-CAVITY SURFACE-EMITTING LASERS FOR OPTICAL COHERENCE TOMOGRAPHY

Bachelor's Thesis
Faculty of Engineering and Natural Sciences
Examiners: Prof. Mircea Guina
Philipp Tatar-Mathes
May 2023

ABSTRACT

Jesse Koskinen: Red-emitting membrane external-cavity surface-emitting lasers for optical coherence tomography
Bachelor's Thesis
Tampere University
May 2023

Optical Coherence Tomography (OCT) has gathered attention as a developing imaging method especially in medicine. It combines the high resolution of confocal microscopy and the imaging depth of ultrasound. However especially at the red spectral range it's lacking suitable light sources. One approach is to use a semiconductor membrane external-cavity surface-emitting laser (MECSEL). In this thesis a red-emitting MECSEL was attempted to realize as a light source for OCT. Different configurations to achieve a suitable light source are investigated.

Keywords: OCT, Michleson interferometer, MECSEL, birefringent filter, etalon

CONTENTS

1. INTRODUCTION

Optical coherence tomography (OCT) has gathered a lot of attention as a developing imaging method during the last years. Applied especially in ophthalmology, OCT systems can produce high quality images with satisfying imaging depth revealing diseases in their earlier stages. There are numerous ways to do OCT with light sources varying from superluminescent diodes implemented in the first systems to complex supercontinuum light sources. It is for sure that lasers have become a fundamental part of today's swept source OCT systems. Recent breakthroughs in laser research enable to build systems with remarkably high resolutions. An interesting option as an OCT light source is to use a semiconductor membrane external-cavity surface-emitting laser (MECSEL) that has been the latest addition to vertically emitting lasers. It has a lot of potential since it can offer a completely new cost-effective solution for an OCT system.

This thesis discusses the theory behind OCT and different ways to build OCT systems. In the second chapter basic theory and fundamental physics behind OCT are described. Different ways to do OCT are introduced and compared. Also various light sources are introduced and their use as a light source for OCT is discussed. In the third chapter MECSELs are introduced and their benefits in OCT are discussed. In the experimental part of this thesis a red-emitting MECSEL was attempted to realize as a potential light source for OCT. The results of the trials are discussed. In the final chapter the results are summarized and a short outlook is taken on to what could be done to further develop MECSELs as potential light sources for OCT.

2. THEORY

2.1 Optical Coherence Tomography

OCT has become a popular imaging method during the last years and is applied mostly in medicine and biomedical optics. It was first demonstrated by Huang *et al.* [1] in 1991. Known to have a lot of potential, it has developed quickly and the amount of publications about OCT is rising rapidly.

OCT is based on measuring the time delay and magnitude of backscattered light [2]. That way information about depth can be obtained. Measuring the echo time delay in a fixed spot is called an A-scan, which can be seen on the left of Fig.2.1. It is performed across the z-axis and gives a one-dimensional data set. By performing sequential A-scans transversely a cross-sectional image can be created which is called a B-scan as in the middle of Fig.2.1. Generating a 3D-image is also possible by performing multiple B-scans utilizing raster scanning. The result of this is called a C-scan as on the right of Fig.2.1. It is beneficial compared to other methods because in it the depth is fixed during every B-scan.

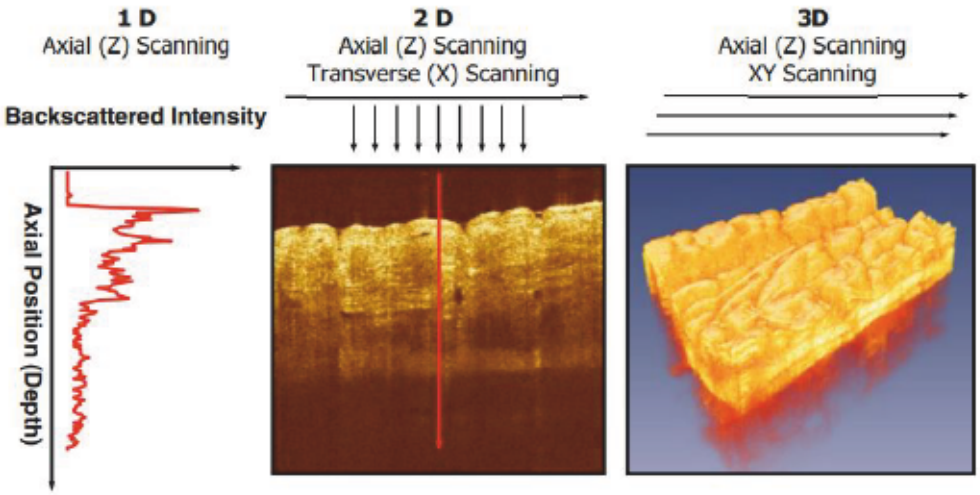

Figure 2.1. *Different scanning methods in OCT (Fig. from [2])*

Resolution and imaging depth are two important parameters in imaging. Figure 2.2 shows how OCT compares to ultrasound and microscopy with respect to these parameters.

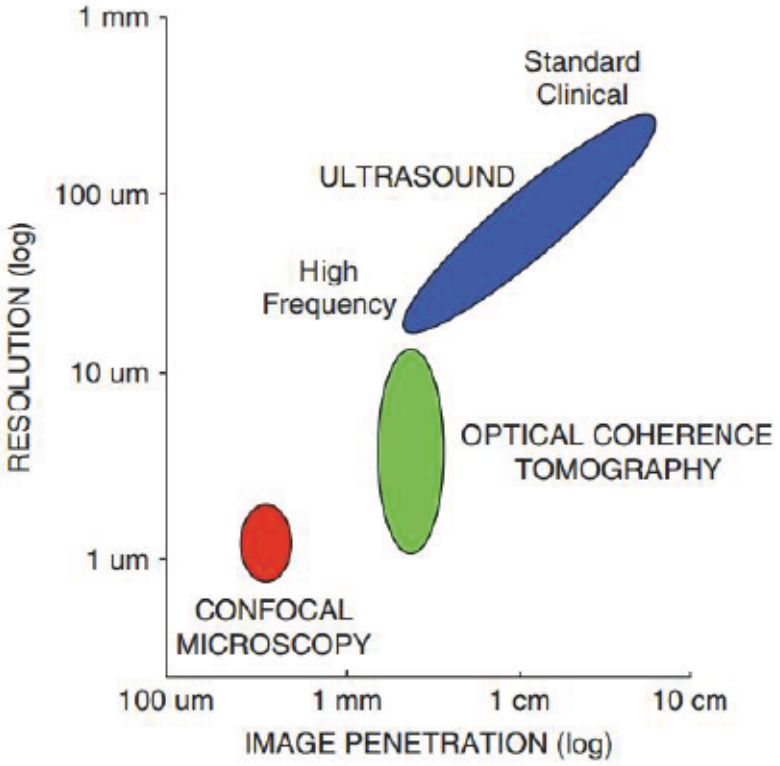

Figure 2.2. *Penetration depth and resolution of OCT, ultrasound and confocal microscopy compared (Fig. from [2])*

As can be seen, OCT is located in the middle filling the gap between microscopy and ultrasound. OCT can reach imaging depths deeper than microscopy but shorter than ultrasound. On the other hand, OCT has an axial resolution of 1 to 10 μm, which is higher than ultrasound but lower than microscopy. In OCT, the axial resolution Δz is the coherence length of the light source. The coherence length is given by:

$$\Delta z = \frac{c}{\Delta f} \tag{2.1}$$

where c is the speed of light and Δf is the frequency bandwidth of the light source. Δf can further be given by:

$$\Delta f = \frac{f \Delta \lambda}{\lambda} \tag{2.2}$$

where f is the central frequency, $\Delta\lambda$ is the spectral bandwidth and λ is the center wavelength of the light source. Substituting 2.2 in 2.1 gives the axial resolution expressed spectrally:

$$\Delta z = \frac{2 \ln 2}{\pi} \cdot \frac{\lambda^2}{\Delta \lambda}. \tag{2.3}$$

In order to have an axial resolution as high as possible, it is necessary to have a light source as broad as possible in a short wavelength range. The penetration depth δ_p can be given when a Fourier transform is executed to the signal in k-space. The result is:

$$\delta_p = \frac{2\ln 2}{\pi} \cdot \frac{\lambda^2}{\delta\lambda} \tag{2.4}$$

where $\delta\lambda$ is the linewidth of the light source. Narrower linewidth enables higher imaging depths but this only applies to swept source OCT which will be discussed later. In general deeper penetration into tissue is possible using wavelengths that are not getting absorbed from water, hemoglobin and melanine. The transverse resolution Δx is given by:

$$\Delta x = \frac{4\lambda}{\pi} \cdot \frac{l}{d} \tag{2.5}$$

where d is the size of the incident beam on the objective lens and l is its focal length. The depth of field b is given by:

$$b = 2z_R = \frac{\pi\Delta x^2}{\lambda} \tag{2.6}$$

where z_R is the Rayleigh range. From equation 2.6 can be seen that higher transverse resolution decreases the depth of field, so there is a trade-off between them. [2]

OCT has advantages compared to other medical imaging technologies because it is non-invasive without the need of harmful radiation, while providing a higher resolution than ultrasound. There is no need for biopsy. Because of this, OCT has successful applications in situations where biopsy is not possible or it has high sampling error. In addition OCT is useful in interventional procedures. Many microsurgeries have been completed using OCT as described by Carrasco-Zevallos *et al.* [3]. Some OCT systems can provide almost real-time OCT scans that gives a base for new applications.

2.2 Michelson Interferometer

OCT uses light to obtain information about depth. However measuring light's time differences is difficult due to its extremely high speed. For example to measure light echoes with a 10 $\mu\mathrm{m}$ resolution a time resolution of 30 fs is required. The time frame is so short that it's impossible to measure it electronically. For that reason some other method must be used. OCT systems have used high-speed optical gating [4], optical correlation [5] and low-coherence interferometry [6]. In this thesis a closer look is taken into interferometry.

OCT systems applying low-coherence interferometry contain a michelson interferometer which is a fundamental part of the system and beneficial in understanding light's be-

haviour. A classic michelson interferometer has a light source from which the incident light is divided into two beams, referred to as a reference beam and a signal beam. The beams are reflected back from mirrors in the interferometer arms and combined. The output $I_D(k)$, often called a spectral interferogram, can be understood by dividing it into three distinct components [2]. Without going into too much detail of the derivation, the first component I_{D1} is called a DC term and is given by:

$$I_{D1} = \frac{\rho}{4}[\, S(k)[\, R_R + R_{S1} + R_{S2} + ...]\,] \tag{2.7}$$

where ρ is the responsivity of the detector, $S(k)$ describes the power spectral dependence of the light source, R_R is the power reflectivity of the reference reflector and $R_{S1}, R_{S2}...$ are sample reflectivities. The second component I_{D2}, called cross-correlation term, is given by:

$$I_{D2} = \frac{\rho}{2}[\, S(k) \sum_{n=1}^{N} \sqrt{R_R R_{Sn}} (cos[\, 2k(z_R - z_{Sn})]\,)] \tag{2.8}$$

where N is the amount of reflections, k is the wave number, z_R is the distance from the beam splitter to the reference reflector and z_S is the path length variable in the sample arm. The final component I_{D3}, called auto-correlation term, is given by:

$$I_{D3} = \frac{\rho}{4}[\, S(k) \sum_{n \neq m=1}^{N} \sqrt{R_{Sn} R_{Sm}} (cos[\, 2k(z_{Sn} - z_{Sm})]\,)]\,. \tag{2.9}$$

The DC term is often the largest component in the signal and causes an offset. The cross correlation term is the most important component for OCT imaging. The square root dependence describes information that enables direct detection of sample reflections. The autocorrelation term appears as artifacts in most OCT systems and the term is wanted to be kept small.

An observation of interference fringes can be obtained with a bare eye by changing the length of the reference arm. Interference fringes will appear as the optical path difference (OPD) changes. Michelson interferometer is shown in Fig. 2.3.

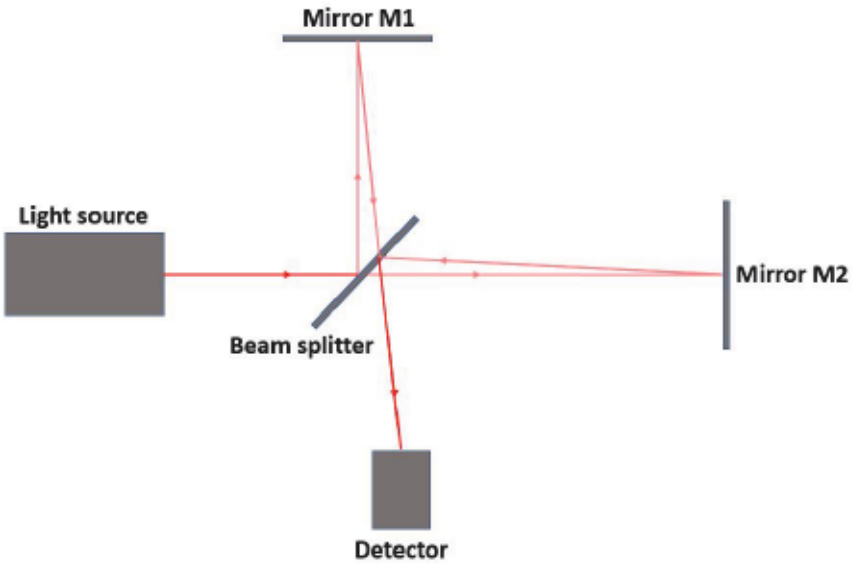

Figure 2.3. Michelson interferometer

Previously, the michelson interferometer has been used to detect gravitational waves [7] and the famous Michelson-Morley experiment was completed using it. In the experiment in 1887 [8], Michelson and Morley tried to prove the existence of a medium called ether that was supposed to carry photons. An interferometer was oriented such that one arm was in the same direction as the earth's rotating direction and the other perpendicular to it. A difference was expected to be seen in the displacement of the interference fringes because the hypothesis was that there would be relative motion between the earth and the ether. However there was barely no change and that concluded that the ether most likely doesn't exist. From the perspectives of Michelson and Morley the experiment was failed but for science it gave a lot of critical information. Later on the experiment has been called one of the most famous failed experiment.

Michelson interferometer is used in several applications. It is a fundamental part in Fourier-transform infrared (FTIR) spectroscopy [9]. FTIR spectrometers are used to obtain emission or absorption spectras. First an interferogram is measured with michelson interferometer and after that it is Fourier transformed into spectral domain, giving information about wavelength. Additionally, the michelson interferometer is used as a standard monitoring tool in cleanroom equipment, for example in inductive coupled plasma etching. It can also be used to measure small surface variations.

In an OCT system the interferometer is slightly modified. The mirror from the signal beam end is removed and the beam is targeted towards a sample being investigated, for example human retina. By scanning through the sample any changes in depth can be seen as the interference fringes start to move and the detected signal changes. In addition fiber-optics can be used in the interferometer. It enables many new applications

such as endoscopic OCT.

2.3 OCT Methods

There are two methods often used in OCT, time domain (TD)-OCT and spectral domain (SD)-OCT [10]. SD-OCT can further be divided into spectrometer based (SB)-OCT and swept source (SS)-OCT.

2.3.1 Time Domain OCT

TD-OCT was used in the first OCT systems. A broadband light source is required and interference is sensed with a photodetector. TD-OCT can be divided into longitudinal TD-OCT and en face OCT. In both cases, the requirement to see interference is that the OPD of the interferometer arms must be less than the coherence length of the light source. Longitudinal TD-OCT is based on moving the reference mirror in the interferometer. By this the correct layer of the sample is selected and the maximum interference is seen when OPD is zero. By scanning the length of OPD, an A-scan is obtained and the photodetector gives a reflectivity profile in depth. From multiple A-scans a cross-sectional B-scan image is formed. Advancing further from multiple B-scans a volumetric image is obtained. In en face OCT the reference mirror is kept at rest and the sample is scanned transversally utilizing T-scans. This way a B-scan is obtained in which the depth is constant. To create a volumetric image (C-scan) from multiple B-scans the reference mirror must be moved slowly axially. En face OCT can be done in real time which is beneficial in medical procedures. A typical TD-OCT system is shown in Fig. 2.4.

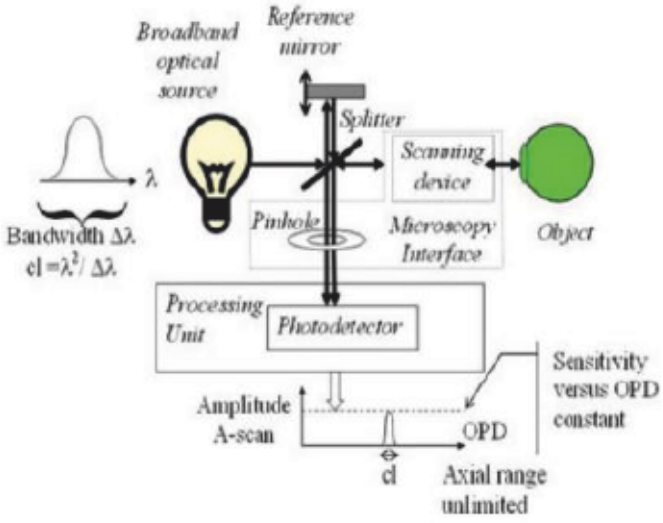

Figure 2.4. *TD-OCT system uses a broadband optical source and a photodetector for signal detection (Fig. from [10])*

Overall TD-OCT is a fast method for creating en face images but for volumetric imaging it is slower because the reference mirror must be moved mechanically.

2.3.2 Spectral Domain OCT

Spectral domain OCT is another method. It has the benefit that all echoes of light at the scanned spot can be measured simultaneously. SB-OCT, like TD-OCT, uses a broadband light source. Detection is done with a spectrometer. Depth information is obtained by first acquiring the intensity signal $I(k)$. It is then fast Fourier transformed (FFT) into frequency domain yielding an A-scan. The limitation in SB-OCT is that developing cameras used in processing units for longer wavelengths is difficult. The camera also sets limits for imaging speeds.

SS-OCT requires light sources that can be swept through spectrally. SS-OCT system has a narrow-bandwidth light source which is frequency tunable. This method is extremely fast because to obtain an A-scan the wavelength range needs to be tuned through only once. It has been reported that SS-OCT is able to produce tuning speeds in the range of MHz [11]. Photodetector is used to detect the signal. Ideally the light source would have infinitesimally narrow linewidth which would lead to a situation where the photodetector signal would look exactly the same in time domain than the original tuning curve in Frequency domain. Similarly than in SB-OCT, intensity signal $I(k)$ is fast Fourier transformed into frequency domain yielding an A-scan. SB-OCT and SS-OCT systems are shown in Fig. 2.5.

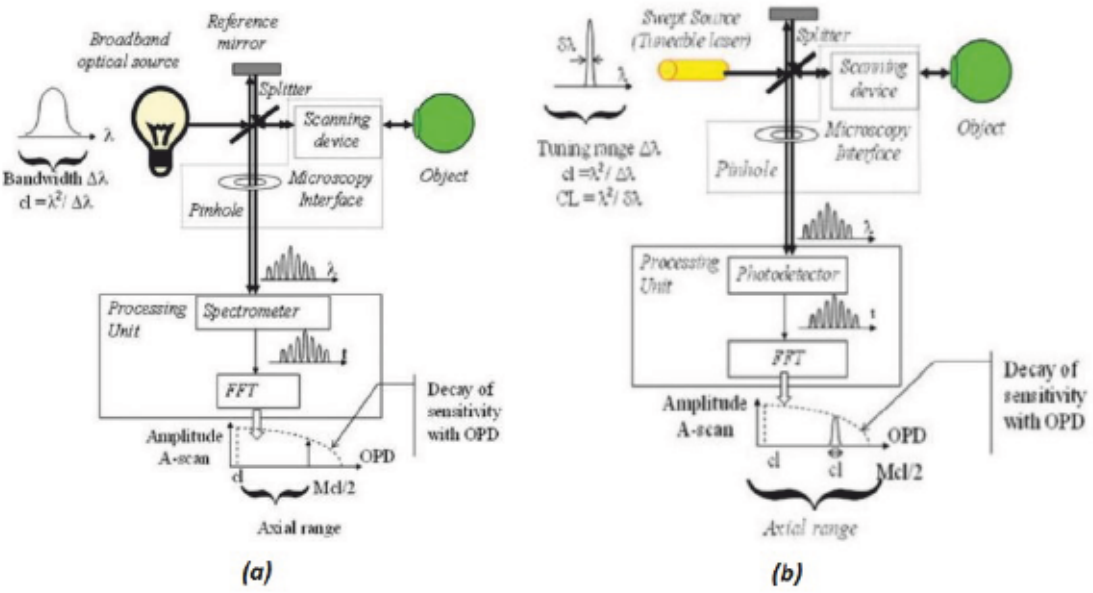

Figure 2.5. *a) SB-OCT system uses a broadband optical source and a spectrometer for signal detection b) SS-OCT system uses a tunable laser source and a photodetector for signal detection (Fig. from [10])*

Within the scope of this thesis, SS-OCT was the method investigated in the experimental part of this thesis.

2.3.3 Comparing The Methods

The main difference between TD-OCT and SD-OCT is that in time domain reflectivity is obtained by varying the length of the reference arm. In spectral domain the length stays fixed and all reflection values for the whole axial range can be obtained at the same reference arm length. This makes SD-OCT faster in scanning through a volume. In [10] it is reported that to aquire a volume of 500 x 500 x 500 pixels at a maximum speed takes 15.5 s in TD-OCT whereas in SS-OCT it takes only 50 µs. However TD-OCT is still slightly faster in producing en face images since in C-scanning the depth is fixed. At maximum speed to create an en face image of 500 lines each consisting of 500 pixels takes 31 µs for TD-OCT compared to 50 µs of SS-OCT.

Another difference is that in spectral domain signal to noise ratio is larger than in time domain. One could assume that with lower powers SD-OCT is able to produce high quality images. Contrarily this is not always the case. As can be seen in the bottom of Fig. 2.5 the amplitude of the signal decreases as the OPD increases. In TD-OCT the amplitude remains constant regardless of the OPD as can be seen in Fig. 2.4. [10]

Focus control differs in SD- and TD-OCT. In SD-OCT it is not possible to synchronize focus control with axial scanning. In TD-OCT it is possible which makes TD-OCT very useful in microscopy applications. The focus can be located exactly where it is desired. However there are still practical issues because it takes relatively long to make a complete scan. For example imaging photoreceptors in the retina is difficult since the patient's eye will move rather quickly during scanning. SD-OCT applications are more attractive for imaging objects in larger scale where a longer distance in depth needs to be in focus simultaneously. For example human retina is suitable for this. [10]

Detectors used in OCT vary depending on the method. TD-OCT uses a photodetector to register changes in interference. This is also the case for SS-OCT. SB-OCT however, uses a spectrometer to register the broadband output. This makes SB-OCT systems expensive. On the other hand SS-OCT systems have high requirements for light sources making them also rather expensive. Overall TD-OCT systems are more cost effective but have weaker performance than SD-OCT systems.

On the application side, SD- and TD-OCT have their own advantages. SD-OCT is especially beneficial in imaging moving organs because of its high imaging speed. For the same reason SD-OCT is used in applications where handheld probes are needed. TD-OCT is more common in applications requiring high transversal resolution because of their feature of having a dynamic focus control.

There are many things to consider while choosing a compatible method to do OCT with. One should always try to choose a method that best suits the specific application.

2.4 OCT Light Sources

The type of light source strongly depends on the OCT application and vice versa. A suitable light source has to meet certain requirements which will be mentioned later on. There needs to be relatively high power, broad spectrum and negligible parasitic spectral modulation [12]. Huang used a superluminescent diode (SLD) emitting at 830 nm central wavelength in his first OCT-system. After that, significant advancements have been reported, including the development of numerous new light sources. Light sources used in OCT include SLDs and swept sources, the latter including supercontinuum (SC) sources and the majority of ultrafast lasers used in OCT.

2.4.1 Superluminescent Diodes

Superluminescent diodes were investigated a lot in the 1980s and 1990s. It lead to their fast development which made it possible to use them in the first OCT systems. SLDs are a suitable option for OCT because they are simple, compact and don't cost a lot. SLDs are placed between LEDs and laser diodes. They emit decent power values with amplified spontaneous emission but never actually lase. In addition their optical spectrum is broad. These features can be achieved using semiconductor laser materials that have high and wide gain spectrum. SLDs range from 670 to 1600 nm and they can have a bandwidth up to 100 nm. For example AlGaAs SLDs have been realized for 780-870 nm and InGaAs SLDs for 920-1060 nm wavelength range [2]. SLD based OCT systems were popular in the 1990s when TD-OCT was widely used. SLDs don't need a cavity like most of the other light sources. This makes SLD based systems more economic. In the future it might be possible to use multi-quantum-well and quantum dot structures that have broad spectrum of over 100 nm and they would give a high 1-2 $\mu\mathrm{m}$ resolution.

2.4.2 Swept Sources

Swept sources for OCT have been researched actively during the last years. Swept sources enable fast imaging. One major advantage of imaging fast is that it becomes possible to image the retina without getting distortions in the image from the patient's movement of the eye; the light source is way faster than that. Unlike SLDs, they do not have a broadband emission but only emit one wavelength at once. The wavelengths are then swept through. In addition to the general requirements mentioned in the beginning of this chapter, the key to make swept sources suitable for OCT is to have a high sweep repetition rate and a narrow linewidth. Fast sweeping results in more reliable imaging and

narrow linewidth improves the coherence length of the light source.

Ultrafast lasers are suitable for OCT because with femtosecond pulses it's possible to achieve high power and broad spectrum. Titanium:Sapphire is a common laser in this category which has been widely applied to OCT systems. Ti:Sa based OCT systems can have a tuning range up to 400 nm emitting at around 800 nm center wavelength. This makes Ti:Sa one of the widest tunable lasers in the world. An example is shown in Fig. 2.6. These conditions result in an axial resolution of less than 1 µm. The disadvantage with Ti:Sa systems is that they require expensive pump sources. Alternatively Cr^{3+} doped LiSAF and LiCAF lasers can be used as solid-state light sources. They offer a tuning range exceeding 150 nm at 850 nm center wavelength and can be pumped with laser diodes at 670 nm. Pulse durations less than 10 fs are possible and the laser system has a resolution less than 2 µm. These features make Cr^{3+} doped LiSAF and LiCAF systems worthy challengers for Ti:Sa systems.

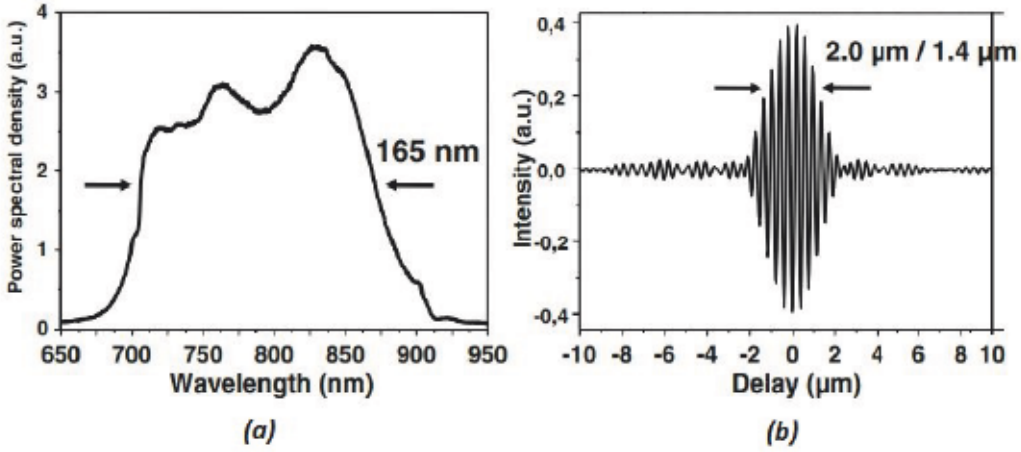

Figure 2.6. *An example of a) an optical output power spectra and b) a corresponding interference signal of a Ti:Sa laser (Fig. from [2])*

OCT has also been carried out using supercontinuum light sources. Most of the visible-light OCT systems feature them. The working principle is that laser output spectrum is widened by nonlinear effects which take place in a photonic crystal fiber. An extremely wide bandwidth [13] is reached enabling resolutions less than a micron. These features make supercontinuum OCT systems extremely fast. Supercontinuum light sources are versatile and can be used for TD-OCT and SD-OCT. Disadvantage with these systems is that the signals contain a lot of noise since keeping ultrashort pulses identical is difficult. Another downside is that the systems are still on research level and expensive.

For swept sources there are plenty of different sweeping methods. Some of them will be considered with more detail in the following. A polygon-based scanning filter contains a grating, a telescope and a polygonal mirror scanner. The polygon mirror rotates fast and all wavelengths are swept through in the space of one plane surface in the polygon. This

configuration is good for making changes with ease. The tuning speed, range, resolution and wavelength can be changed by controlling the filter components. The disadvantage comes with the polygonal mirror since it's relatively big and moves constantly. With this method linewidths less than 0.1 nm, sweep rates faster than 115 kHz and tuning ranges over 150 nm have been realized. The filter system is shown in Fig. 2.7.

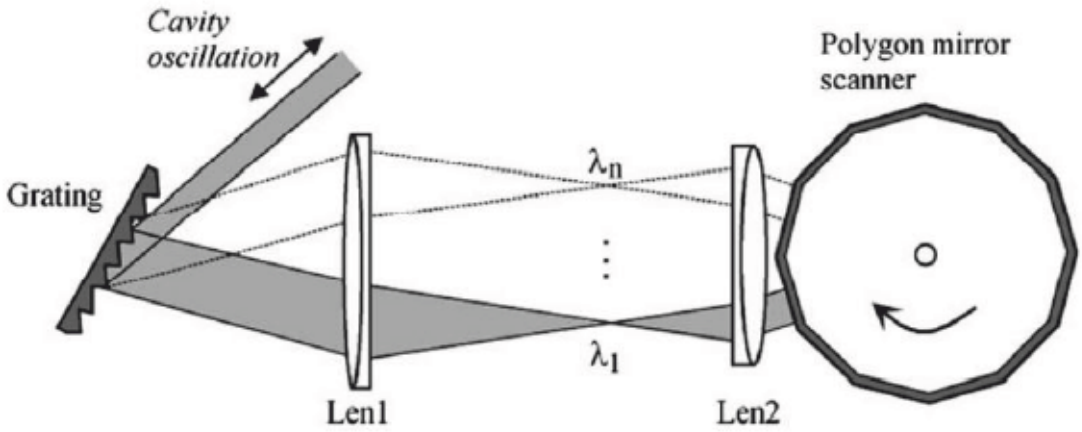

Figure 2.7. *Schematic of a polygon-based scanning filter (Fig. from [2])*

Some systems use a Fabry-Perot tunable etalon. It contains two highly reflecting mirrors that are close to each other. Their distance is changed with a piezoelectric actuator. It is possible to achieve sweep rates of hundreds of kHz. Unlike the polygon-based scanning filter, Fabry-Perot etalon doesn't take that much space but it has a disadvantage due to a nonlinear tuning curve.

There are also other potential possibilities for sweeping. For example cavities that have gratings could provide fast sweeping if the end mirror is mounted on a resonant micro-electro-mechanical system (MEMS). Using a MEMS would allow compact systems because it is integrated with a semiconductor gain chip directly. Commercially this is very attractive. Another option is to use intracavity elements such as an etalon to narrow down the linewidth and a birefringent filter for sweeping. This will be discussed later in the thesis.

Systems containing a MEMS can be integrated with a semiconductor vertical cavity surface emitting laser (VCSEL). VCSELs have epitaxially grown multi-quantum well gain region between two distributed bragg reflector (DBR) mirrors. In a MEMS-VCSEL the other DBR mirror is replaced with a dielectric mirror which is separated from the chip with an air gap. The air gap is varied with a MEMS. MEMS-VCSELs would fix the main issues that swept sources have always had. They don't have a restricted fixed sweep rate and the dynamic coherence length is not limited by multimode operation. In the mid 2010s MEMS-VCSELs started to become more common in industry.

3. MEMBRANE EXTERNAL-CAVITY SURFACE-EMITTING LASER

3.1 MECSEL vs Other Semiconductor Laser Diodes

In this work a MECSEL was attempted to use as a light source for OCT. MECSELs are one of the latest innovations in surface-emitters [14]. They have developed from vertical-external-cavity surface emitting lasers (VECSELs) [15] that are a continuity from VCSELs. A MECSEL's gain chip consists only of an active region. Quantum wells (QW) in the active region are excited and provide gain by stimulated emission. The chips are grown by molecular beam epitaxy (MBE) which is a common epitaxy method used in manufacturing semiconductor devices. The MECSEL's gain chip architecture is beneficial since there are no DBRs that have a finite stop band meaning it is possible to grow structures for wavelengths that were difficult to realize before. In semiconductor lasers there are spectral gaps and a lack of high-power devices at certain wavelengths. For example spectral regions from $460\mathrm{nm}$ to $620\mathrm{nm}$ and from $1350\mathrm{nm}$ to $1540\mathrm{nm}$ are represented weakly [16]. These wavelengths can be reached with second harmonic generation but that adds costs to the laser system. In the future these gaps could potentially be filled with MECSELs. Besides access to novel wavelengths, the lack of DBRs enable the use of two intra-cavity heat spreaders which makes heat extraction exceptional compared to other semiconductor laser diodes. Common heat spreader materials used are sapphire, silicon carbide (SiC) and diamond with diamond having the highest thermal conductivity of $2000\mathrm{W}/(\mathrm{m}\cdot\mathrm{K})$ [17]. Simulations have shown that the membrane temperature decreases up to a factor of two with SiC and diamond heat spreaders and with sapphire the temperature reduction can be up to a factor of four [18]. Fig.3.1a shows a simulation about MECSEL's thermal behaviour and demonstrates that MECSELs have a very homogeneous and effective heat distribution. DBRs have two orders of magnitude worse thermal conductivity than diamond making thermal management a major benefit in MECSELs. Another benefit is that the gain chip can be double-side pumped resulting in a more homogeneous charge carrier density. This results in lower lasing threshold and an increased differential efficiency. Power scaling to higher powers is possible. Double-side pumping is particularly beneficial for gain membranes thicker than $625\mathrm{nm}$ [18]. Since being a surface-emitting laser, MECSELs have a built-in feature of having a great beam

quality in the region of $M^2 < 1.06$ as described in [16]. A typical gaussian beam profile of a MECSEL is shown in Fig.3.1b.

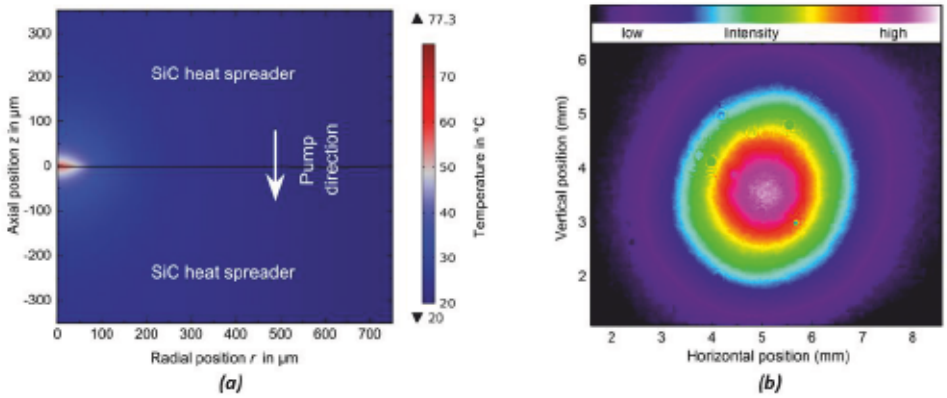

Figure 3.1. *a) A cross-sectional view of a MECSEL gain membrane bonded between two SiC heat spreaders with simulated temperature. A very homogeneous heat distribution is achieved b) MECSEL beam has a gaussian intensity distribution with* $M^2 < 1.06$ *(Fig. a from [18] and Fig. b from [14])*

Having access to novel wavelengths combined with effective thermal management make MECSELs attractive in the semiconductor laser market. MECSELs can provide a cost-effective option for future applications since there are no need for expensive pump sources or complex DBR structures.

To achieve lasing, an external cavity is formed around the gain membrane. A schematic of a MECSEL operating in a linear cavity is shown in Fig.3.2.

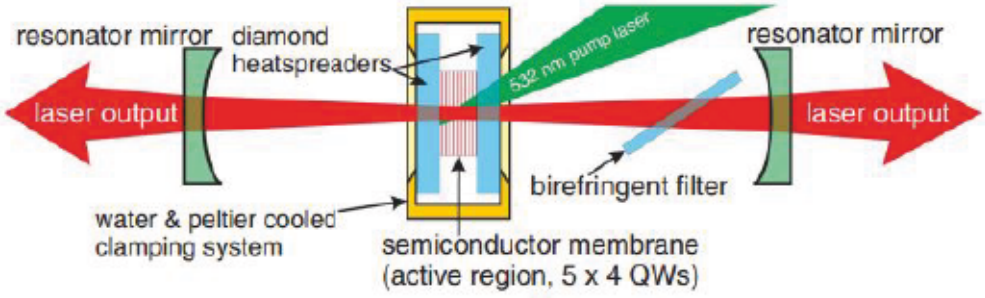

Figure 3.2. *Schematic of a MECSEL in a linear cavity configuration (Fig. from [16])*

From Fig.3.2 can be seen that the semiconductor membrane is bonded between two diamond heat spreaders and mounted on a water cooled heat sink. Two external dielectric mirrors are used to form the cavity. The structure can be optically pumped from the sides and in the right conditions lasing occurs. Usually one mirror is highly reflective (R>99%) and the other one lets through a bit more from where the light is then coupled out.

MECSELs have developed a lot in the recent years and they have been realized for a wide variety of wavelengths. For example MECSELs emitting at around 650 nm [14], 800 nm [19], 1 µm [20] and 1.5 µm [21] have been demonstrated. The fast development has led to new application ideas, such as using MECSELs in guide stars [22]. One option is to attempt a red-emitting MECSEL in OCT. Red spectral range is interesting because its water absorption coefficient is very low [23] meaning it's easier to penetrate through tissue. The effects of water absorption and spectral bandwidth on axial resolution are shown in Fig.3.3.

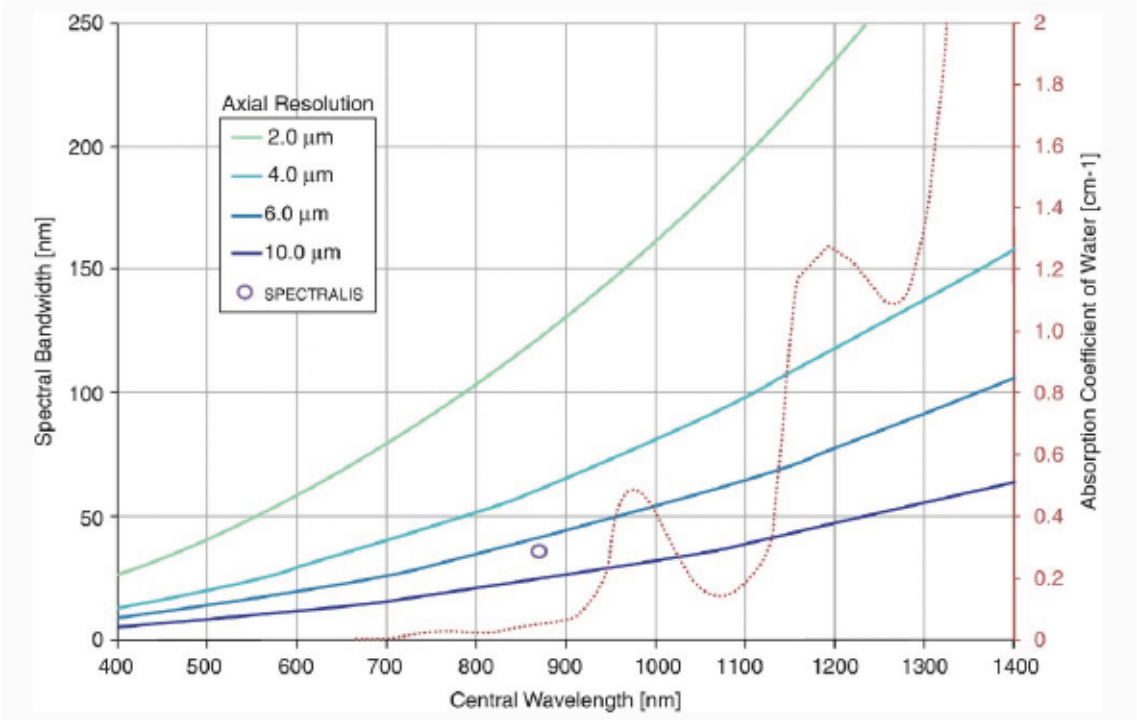

***Figure 3.3.** A graph showing how water absorption and spectral bandwidth affect the axial resolution in OCT (Fig. from [23])*

Based on previous publications, MECSELs could be a potential light source for OCT. They can produce a wide enough tuning range of more than 10 nm with a minimum output power of 5 mW through the tuning range. Using a motorized stage the tuning speed can exceed 1 kHz.

3.2 Principles of Operation

One of the benefits MECSELs have is that they operate in an open cavity. It enables the use of intracavity elements that can be helpful in applications. OCT requires a narrow linewidth and a wide tuning range. With MECSELs this is possible to achieve by using an etalon and a birefringent filter as intracavity elements. They narrow down the linewidth and in addition birefringent filter makes spectral tuning possible.

3.2.1 Birefringent Filter

A birefringent filter can be used in laser resonators for tuning and narrowing down the linewidth. Its working principle is based on interference that occurs when polarized light is transmitted through the layers of a birefringent crystal [24]. This creates losses spectrally and the laser operates near the minimum losses. By rotating the birefringent filter the spectral area where the minimum losses are shifts and the laser operates at a different wavelength. The transmission spectrum is determined by the material and thickness of the birefringent crystal. Transmission is given by [25]:

$$T = [A' \cdot \frac{\sin(2^N \theta)}{2^N} \cdot \sin\theta]^2 \tag{3.1}$$

where A' is the amplitude, N is the amount of plate filters and θ is given by:

$$\theta = \frac{\pi(n_e - n_o)d}{\lambda} \tag{3.2}$$

where d is the thinnest plate's thickness, n_e and n_o are the ordinary and extraordinary indices of the birefringent crystal and λ is the wavelength. Increasing the thickness of the crystal results in more narrow peaks that are closer to each other. To narrow down the linewidth even more, multiple crystals can be stacked together.

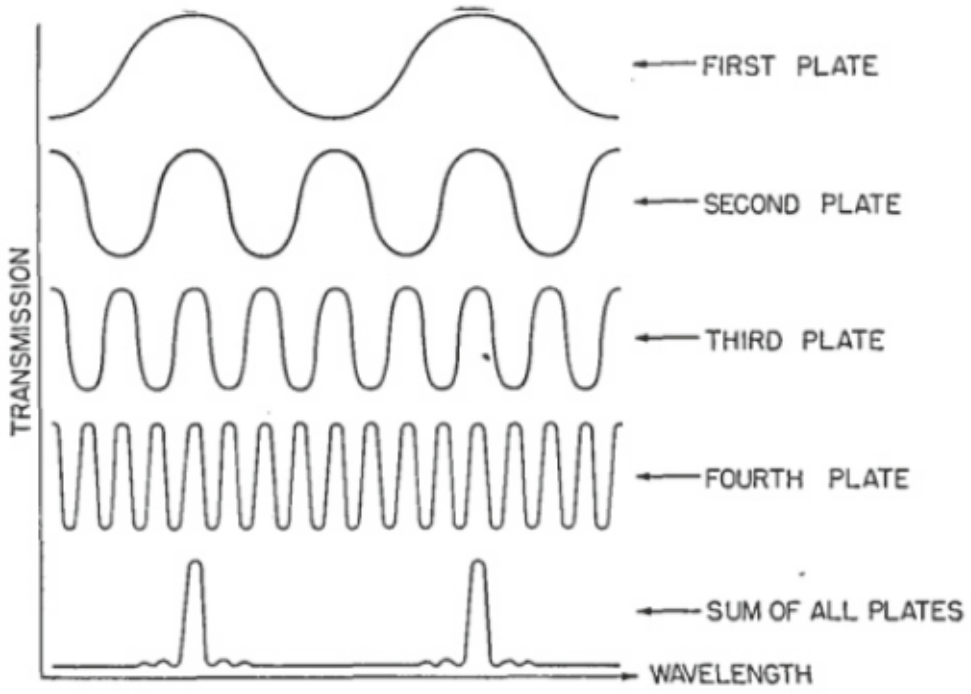

Figure 3.4. *Transmission sepctrum for multiple birefringent crystal plates oriented parallel to each other (Fig. from [25])*

Transmission spectrums for different thicknesses of birefringent crystal plates can be seen in Fig. 3.4 with the first plate being the thinnest and the fourth plate being the thickest. The sum spectrum of all four plates stacked together parallel to each other shows that the thinnest crystal plate decides the spectral separation of the transmission maximas and the thickest crystal plate the linewidth of a single transmission peak. Birefringent filters are widely used in optical systems where quartz is the most common material.

3.2.2 Etalon

Besides the birefringent filter, an etalon is another way to narrow down the linewidth. An etalon is a Fabry Perot instrument that was developed by Charles Fabry and Alfred Perot in 1899 [26]. It can be a transparent plate or it can consist of two mirrors that have an air gap between them. In a cavity they act as optical resonators and their transmissivity varies with the optical frequency. Common materials used are fused silica, germanium and YAG. Etalons can be compared by calculating a finesse factor F for them, which describes an optical resonator. Finesse is beneficial for comparison because it is independent of the resonator's length or other geometrical properties. Finesse is defined by the relation between free spectral range (FSR) and linewidth of the resonances. FSR is the separation of resonator modes and is given by:

$$\Delta\nu = \frac{c}{2nL} \tag{3.3}$$

in which n is the refractive index and L is the resonator length. There are different expressions for finesse in literature but according to [27] an exact expression for the finesse of an ideal optical cavity is given by:

$$F = \frac{2R}{(1-R)^2} \tag{3.4}$$

in which R is the intensity reflectivity of the cavity mirrors. Higher finesse factor corresponds to resonances that are sharp and separated by a longer distance.

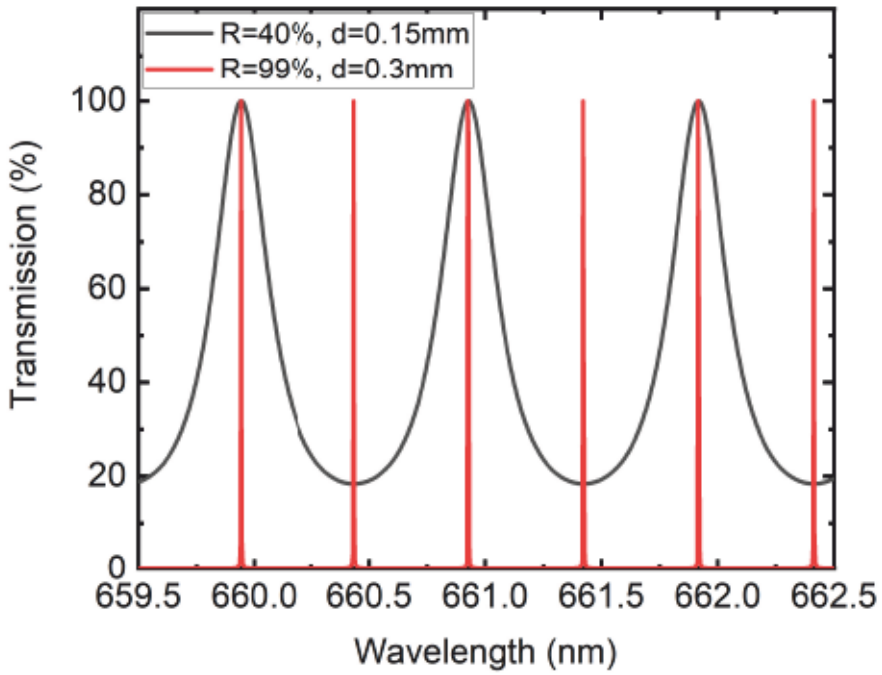

Figure 3.5. *Behaviour of an air gap etalon with varying reflectivity and distance*

Fig. 3.4 shows the behaviour of an air gap etalon made of two fused silica plates. Reflectivity R and distance between the plates d are varied. Higher reflectivity reduces linewidth while longer distance between the plates reduces the free spectral range. In the end there is a trade off between the etalon and the resonator to provide narrow linewidth with a sufficient gain.

4. EXPERIMENTAL

4.1 Setup

The aim of the experimental part of this thesis was to provide a suitable light source for OCT that could execute A-scans. As mentioned before in the thesis, based on earlier research MECSEL satisfyes most of the requirements for an OCT light source. The power is sufficient, gain spectrum is broad, sweeping can be made fast and the linewidth can be made narrow. The semiconductor structures were based on AlGaInP material system. A structure containing 10 packages and another containing 5 packages of quantum wells were attempted. Each package contained 4 single QWs. The sample with 5 QW packages performed better and all the results shown here were achieved with it.

The semiconductor structure was sandwiched between two diamond heat spreaders and placed in a water cooled copper mount. The sample was then deployed to a z-cavity configuration. The illustration of the setup can be seen in Fig. 4.1.

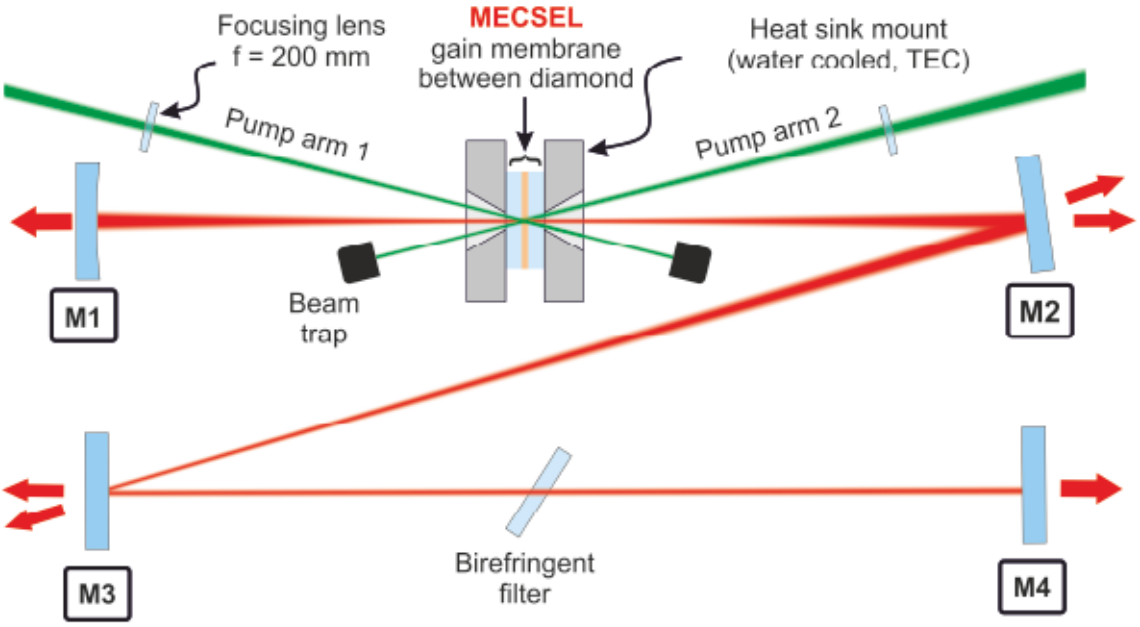

Figure 4.1. *MECSEL operating in a Z-cavity. The gain membrane was coated to have a 40% reflectivity and acted as an etalon. With this setup the best results were reached*

The gain membrane was pumped from both sides with a Coherent Verdi V-6 laser. Its

emission wavelength is 532 nm and capable to produce pump powers up to 6.5 W. The pump beams were focused down to the membrane by using 200 mm plano-convex lenses in pump arms. Beam traps behind the copper mount were used to catch the transmitted pump beams. A z-cavity was built around the gain membrane. This configuration was chosen because the birefringent filter would be more practical to use. Four dielectric mirrors were used to form the cavity. All mirrors were highly reflective, M1 being the outcoupler with a focal length of 150 mm. M2 had a focal length of 250 mm, while M3 and M4 were plane mirrors. The output beam from M1 was collimated and directed to a michelson interferometer.

The interferometer consisted of a Thorlabs CCM1BS014/M non-polarizing beam splitter that split the beam towards two dielectric mirrors, other one being a reference mirror and the other a signal mirror. Beams reflecting back from the mirrors were combined in the beamsplitter and headed towards a photodetector which registered the interference signal. When holding a white paper in front of the photodetector, interference fringes were visible. Changing the reference arm length caused the fringes to move as expected.

4.2 Tuning

The MECSEL was tuned by rotating a 2 mm thick quartz birefringent filter inside the cavity. Filters with different thicknesses and stacks of more than one filter were attempted with the 2 mm filter having the best tuning range. The filter was placed at Brewster's angle to minimize reflection losses. It was controlled by a Thorlabs KBD101 motorized stage. Swept sources in OCT require fast sweeping to make picture forming more efficient and realiable. The stage can reach velocities up to 100 $\mathrm{mm/s}$ which is sufficient enough for an OCT light source. The tuning measurement was performed by recording multiple spectras separately. The birefringent filter was first rotated to the shortest possible wavelength where the laser operates. The spectra was recorded and after that the filter was rotated slightly which caused the wavelength to shift to a longer one. The spectra at the new spot was recorded and the same procedure was repeated until the laser could not operate anymore. The MECSEL gave a tuning range of around 18 nm from 652 nm to 670 nm with a sufficient minimum power of 5 mW. The tuning measurement can be seen in Fig. 4.2. The spectras were recorded with an Optical Spectrum Analyzer that had a resolution of 0.25 nm.

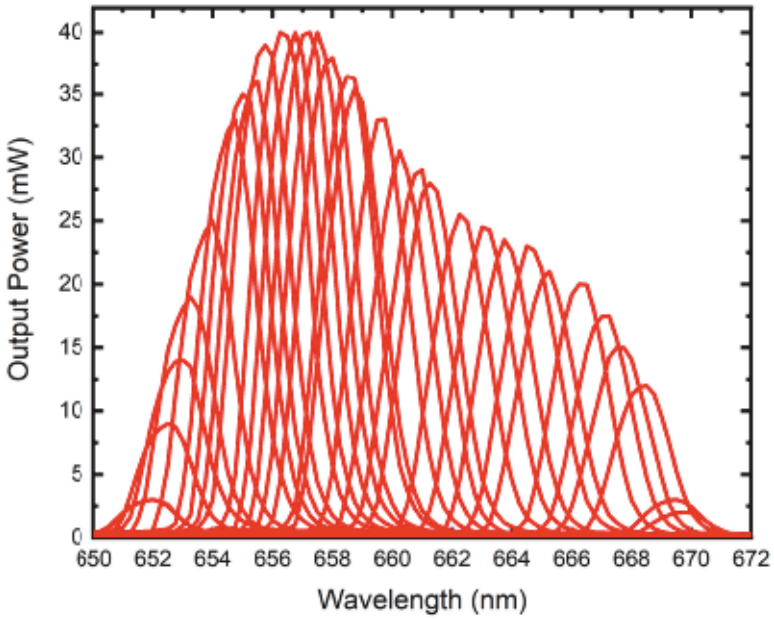

Figure 4.2. *A tuning range of 18* nm *using a 2* mm *thick birefringent filter was achieved from the MECSEL*

Besides tuning it's important to review the linewidth of a single emission peak. Narrower linewidth together with red spectral area corresponds to a deeper penetration depth as can be seen from Eq.2.4. For this MECSEL the objective was to have a linewidth of less than 0.1 nm that would correspond to a penetration depth of around 2 mm. Fig. 4.3 shows an emission spectrum of a MECSEL with a 2 mm birefringent filter inside the cavity. The spectrum is a single emission peak from Fig. 4.2.

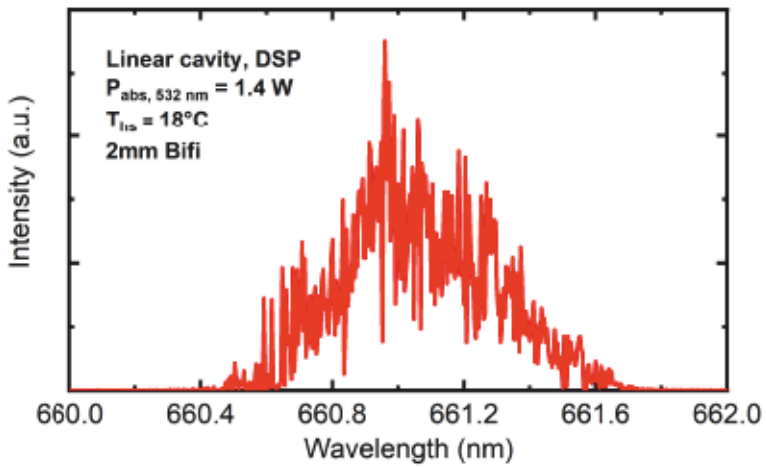

Figure 4.3. *Zooming into a single emission peak shows the birefringent filter's effect on the linewidth which is now around 0.6* nm

The implementation of a birefringent filter resulted in an emission linewidth of about 0.6 nm. This is too large for an implementation into OCT, as it would only allow for an axial range of 0.32 mm. An additional etalon inside the cavity can further narrow down the linewidth. There were multiple attempts to find a suitable etalon. One approach was to use a Fabry-Perot etalon consisting of two wedged fused silica plates separated by an air gap. This would have been the most convenient way for the OCT system because sweeping could have been done by only changing the minor gap between the fused silica plates. In practise lasing was difficult to achieve. First of all the wedged fused silica plates had to be parallel to each other with a difference of 180 degrees in their orientation. Besides that the whole Fabry-Perot etalon had to be perfectly aligned in the cavity. After several attempts lasing was achieved with this approach as can be seen in Fig.4.4. However the Fabry-Perot etalon introduced too much losses in the cavity leading to a limited output power and tuning range.

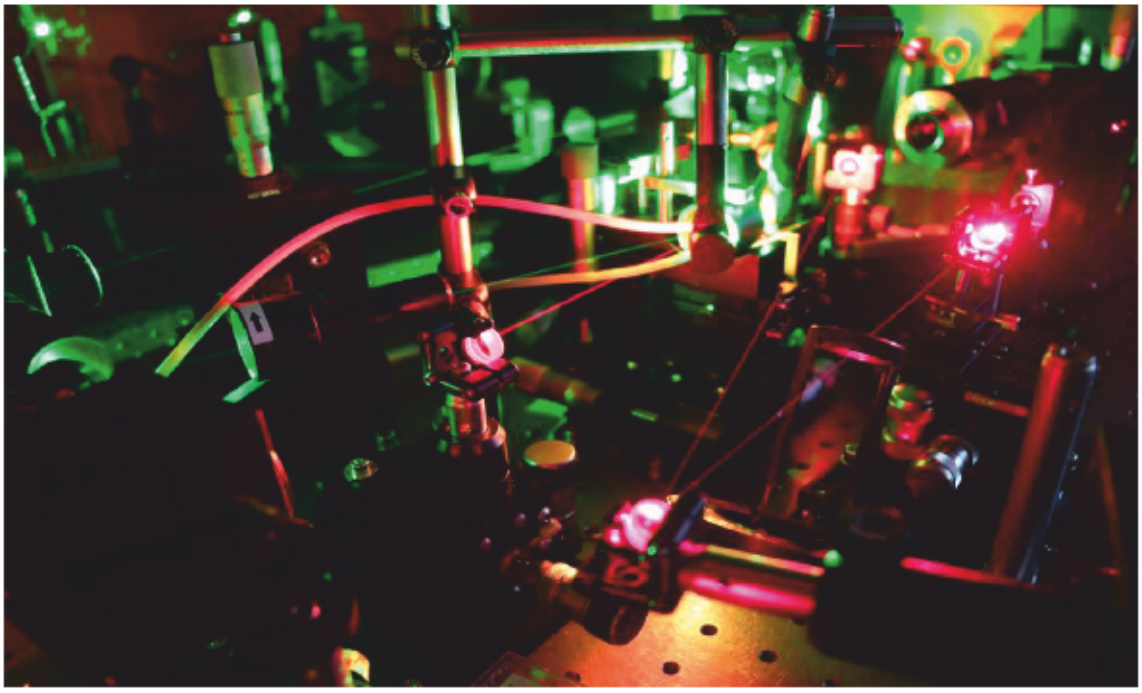

Figure 4.4. *A MECSEL with a Fabry-Perot etalon operating in a z-cavity. The Fabry-Perot etalon and the birefringent filter can be seen on the right side of the figure*

Another approach was to use two birefringent filters inside the cavity. This was attempted with different combinations. The main idea was to keep one filter fixed and tune the laser with the other one. With this approach the laser had too much losses and the linewidth was not narrow enough. The next approach was to coat the sandwiched membrane to act as an etalon. It came out to be the best solution. The membrane was coated so that it had a 40% reflectivity corresponding to a finesse factor of 2.2 according to Eq.3.4. This way the etalon effect of the heat spreaders was cancelled out. After this the spectrum of a single emission peak was measured again, this time with an Optical Spectrum Analyzer

that had a resolution of 0.02 nm. The spectrum got more narrow as can be seen from Fig. 4.5.

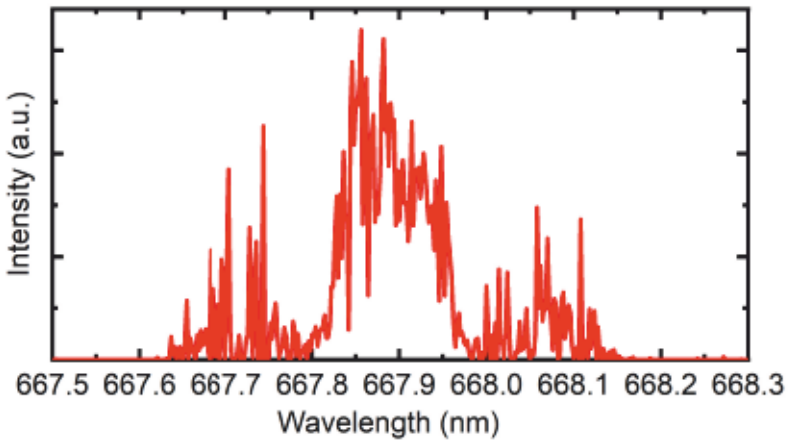

***Figure 4.5.** After coating the MECSEL sandwich to act as an etalon the linewidth got more narrow*

The linewidth of a single emission peak is less than 0.2 nm which is very close to the 0.1 nm objective. However there are three laser modes operating simultaneously. It caused the observed photodetector signal to have a lot of background noise making reliable OCT measurements impossible. The issue could be fixed by only having one laser mode active at a time. This could be achieved in the future but more research needs to be carried out. One option would be to try more iterations with different birefringent filter and etalon combinations. Another interesting approach to reach single-frequency operation would be to attempt active stabilization. This has already been demonstrated for VECSELs [28] and a schematic of the setup is shown in Fig.4.6.

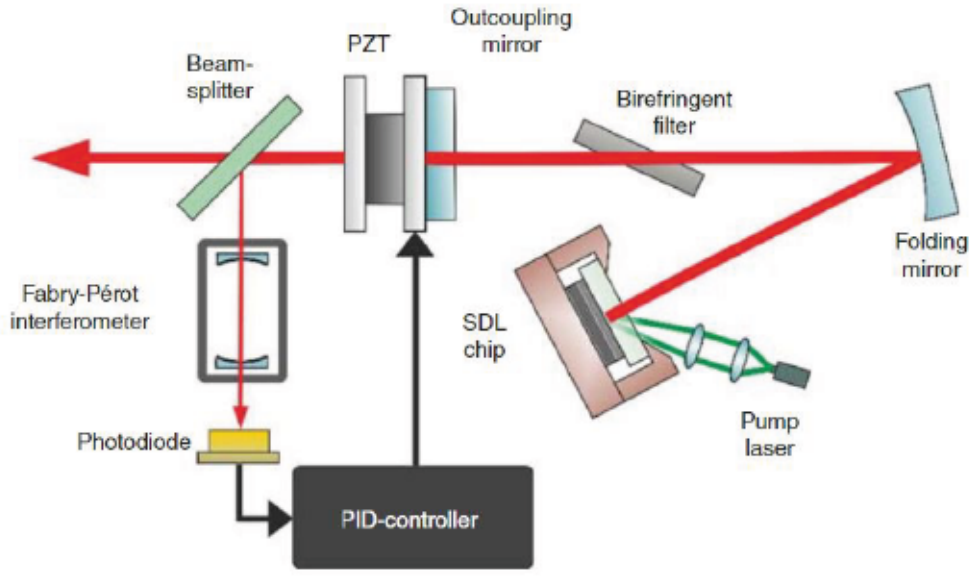

***Figure 4.6.** An example of active stabilization used in VECSELs (Fig. from [28])*

The main idea in this type of active stabilization is to include a passive cavity in the system, for example a Fabry-Perot interferometer. Any wavelength changes in the laser appear as an intensity change of the output in the Fabry-Perot interferometer. This creates an error signal that causes a change in the cavity length to stabilize the laser wavelength. Movement of the cavity mirror is achieved with a piezoelectric material in which the mirror is mounted. A completely new perspective would be to use the gain membrane as an optically pumped edge emitter. This could potentially give huge benefits.

5. CONCLUSION

OCT is a developing imaging method that can be realized in different ways. Many OCT systems rely on low-coherence interferometry which is a fundamental part of today's physics. It's always important to choose the best method and light source regarding the OCT application. An interesting option is to use a MECSEL that has potential for a high-quality OCT light source.

The experimental part of this thesis aimed to realize a red-emitting MECSEL as a light source for OCT. The MECSEL gave a tuning range of 18 nm with a minimum power of 5 mW. Narrowing down the laser's linewidth came out to be the biggest obstacle. With the coating of the MECSEL itself with a slightly higher reflective coating, this problem could be fixed. The issue arises from fast tuning while having active frequency stabilization. Applying a 2 mm birefringent filter to the cavity and coating the membrane to act as an etalon with a 40% reflectivity gave the best outcome. With this configuration the linewidth reduced to be less than 0.2 nm. However there were multiple laser modes operating simultaneously that caused too much background noise in the observed photodetector signal, making realiable OCT impossible.

In the future more work needs to be done to make MECSELs realiable light sources for OCT. Frequency stabilization is needed and can be achieved by iterating more between different birefringent filter and etalon combinations. Another approach would be to utilize feedback loops that control the cavity mirrors forcing the laser to single mode operation or to use the gain membrane as an optically pumped edge emitter that can also give huge benefits.

REFERENCES

[1] D. Huang et al. “Optical Coherence Tomography”. In: *Science* 254.5035 (1991), pp. 1178–1181. DOI: 10.1126/science.1957169.

[2] W. Drexler and J. G. Fujimoto. *Optical coherence tomography*. Springer Cham, 2015.

[3] O. M. Carrasco-Zevallos et al. “Review of intraoperative optical coherence tomography: technology and applications”. In: *Biomed. Opt. Express* 8.3 (2017), pp. 1607–1637. DOI: 10.1364/BOE.8.001607.

[4] M. W. Jenkins et al. “In vivo gated 4D imaging of the embryonic heart using optical coherence tomography”. In: *Journal of Biomedical Optics* 12.3 (2007), p. 030505. DOI: 10.1117/1.2747208.

[5] S. Moon, Y. Qu, and Z. Chen. “Characterization of spectral-domain OCT with autocorrelation interference response for axial resolution performance”. In: *Opt. Express* 26.6 (2018), pp. 7253–7269. DOI: 10.1364/OE.26.007253.

[6] D. Huang et al. “Micron-resolution ranging of cornea anterior chamber by optical reflectometry”. In: *Lasers in Surgery and Medicine* 11.5 (1991), pp. 419–425. DOI: https://doi.org/10.1002/lsm.1900110506.

[7] B. P. Abbott et al. “GW151226: Observation of Gravitational Waves from a 22-Solar-Mass Binary Black Hole Coalescence”. In: *Phys. Rev. Lett.* 116 (24 2016). DOI: 10.1103/PhysRevLett.116.241103.

[8] A. A. Michelson and E. W. Morley. “On the relative motion of the Earth and the luminiferous ether”. In: *American Journal of Science* s3-34.203 (1887), pp. 333–345. DOI: 10.2475/ajs.s3-34.203.333.

[9] P. R. Griffiths and J. A. de Haseth. *Fourier Transform Infrared Spectrometry*. John Wiley Sons, Ltd, 2007. Chap. 2.

[10] A. Gh. Podoleanu. “Optical coherence tomography”. In: *Journal of Microscopy* 247.3 (2012), pp. 209–219. DOI: https://doi.org/10.1111/j.1365-2818.2012.03619.x.

[11] W. Wieser et al. “Multi-Megahertz OCT: High quality 3D imaging at 20 million A-scans and 4.5 GVoxels per second”. In: *Opt. Express* 18.14 (2010), pp. 14685–14704. DOI: 10.1364/OE.18.014685.

[12] X. Shu, L. J. Beckmann, and H. F. Zhang. “Visible-light optical coherence tomography: a review”. In: *Journal of Biomedical Optics* 22.12 (2017), pp. 1–14. DOI: 10.1117/1.JBO.22.12.121707.

[13] B. Kuyken et al. “Octave-spanning coherent supercontinuum generation in an AlGaAs-on-insulator waveguide”. In: *Opt. Lett.* 45.3 (2020), pp. 603–606. DOI: 10.1364/OL.45.000603.

[14] H. Kahle et al. “Semiconductor membrane external-cavity surface-emitting laser (MECSEL)”. In: *Optica* 3 (2016), pp. 1506–1512. DOI: 10.1364/OPTICA.3.001506.

[15] M. Kuznetsov et al. “High-power (>0.5-W CW) diode-pumped vertical-external-cavity surface-emitting semiconductor lasers with circular TEM/sub 00/ beams”. In: *IEEE Photonics Technology Letters* 9.8 (1997), pp. 1063–1065. DOI: 10.1109/68.605500.

[16] H. Kahle. “AlGaInP-based high-performance semiconductor disk lasers for the red spectral range: Gain chip design, harmonic generation and a new laser concept”. PhD thesis. 2016.

[17] H.-M. Phung et al. “Thermal Behavior and Power Scaling Potential of Membrane External-Cavity Surface-Emitting Lasers (MECSELs)”. In: *IEEE Journal of Quantum Electronics* 58.2 (2022), pp. 1–11. DOI: 10.1109/JQE.2022.3147482.

[18] H.-M. Phung. “Semiconductor membrane external-cavity surface-emitting lasers (MECSELs) : power scaling, thermal management, and wavelength extension”. PhD thesis. 2021.

[19] H. Kahle et al. “Comparison of single-side and double-side pumping of membrane external-cavity surface-emitting lasers”. In: *Opt. Lett.* 44.5 (2019), pp. 1146–1149. DOI: 10.1364/OL.44.001146.

[20] H. Kahle et al. “Membrane external-cavity surface-emitting lasers for high power broadband emission in the 1 µm range”. In: *2021 27th International Semiconductor Laser Conference (ISLC)*. 2021, pp. 1–2. DOI: 10.1109/ISLC51662.2021.9615904.

[21] H.-M. Phung et al. “Quantum dot membrane external-cavity surface-emitting laser at 1.5 µm”. In: *Applied Physics Letters* 118.23 (2021), p. 231101. DOI: 10.1063/5.0053961.

[22] D. Priante et al. “Demonstration of a 20-W membrane-external-cavity surface-emitting laser for sodium guide star applications”. In: *Electronics Letters* 57.8 (2021), pp. 337–338. DOI: https://doi.org/10.1049/ell2.12008.

[23] J. F. Bille. “Optical Coherence Tomography (OCT): Principle and Technical Realization”. In: *High Resolution Imaging in Microscopy and Ophthalmology: New Frontiers in Biomedical Optics*. Springer, 2019. Chap. 3, pp. 59–85. DOI: 10.1007/978-3-030-16638-0.

[24] J. W. Evans. “The Birefringent Filter”. In: *J. Opt. Soc. Am.* 39.3 (1949), pp. 229–242. DOI: 10.1364/JOSA.39.000229.

[25] B. H. Billings. “A Tunable Narrow-Band Optical Filter”. In: *J. Opt. Soc. Am.* 37.10 (1947), pp. 738–745. DOI: 10.1364/JOSA.37.000738.

[26] A. Perot and C. Fabry. “On the Application of Interference Phenomena to the Solution of Various Problems of Spectroscopy and Metrology”. In: *The Astrophysical Journal* 9 (1899).

[27] M. Suter and P. Dietiker. “Calculation of the finesse of an ideal Fabry-Perot resonator”. In: *Appl. Opt.* 53.30 (2014), pp. 7004–7010. DOI: 10.1364/AO.53.007004.

[28] M. Rattunde, P. Holl, and J. Wagner. “Single-frequency and High Power Operation of 2–3 Micron VECSEL”. In: *Vertical External Cavity Surface Emitting Lasers*. John Wiley Sons, Ltd, 2021. Chap. 3, pp. 63–107. DOI: https://doi.org/10.1002/9783527807956.ch3.